RESEARCH OUTPUTS / RÉSULTATS DE RECHERCHE

Cross section measurements of the ^{1}H(^{3}He,^{1}H)^{3}He reaction at 20° and 30° between 1.9 and 3.0 MeV

Terwagne, Guy; Ross, Guy G.; Leblanc, Luc

[Link to publication](#)

Cross section measurements of the ^{1}H(^{3}He,^{1}H)^{3}He reaction at 20° and 30° between 1.9 and 3.0 MeV

G. Terwagne[a)]
LARN, Facultés Universitaires Notre-Dame de la Paix, 22 rue Muzet, B-5000 Namur, Belgium

G. G. Ross and L. Leblanc
INRS-Energie et Matériaux, Université du Québec, C.P. 1020, Varennes, Québec J3X IS2, Canada

The cross sections of the ^{1}H(^{3}He,^{1}H)^{3}He reaction have been measured at two different angles (20° and 30°) for ^{3}He particles incident energies between 1.9 and 3.0 MeV. This reaction offers an alternative to the classical ^{1}H(^{4}He,^{1}H)^{4}He elastic recoil reaction and can be more attractive because ^{3}He incident particles induce nuclear reactions on light elements such as ^{12}C, ^{14}N, or ^{16}O. The new technique has been applied to silicon implanted with low energy hydrogen as well as a C$_x$H$_y$/Cu/Cu$_x$H$_y$/Si specimen. For this multilayer, carbon, hydrogen, and carbon can be analyzed together using three different charge particle detectors. © *1996 American Institute of Physics.*
[S0021-8979(96)01512-5]

I. INTRODUCTION

Profiling hydrogen using elastic recoil detection (ERD) induced by ^{3}He particles is not very usual. Alpha particles are often preferred to other particles due to the fact that nuclear reactions induced by these particles is almost elastic scattering. Nevertheless, ^{3}He particles induce nuclear reactions on light elements such as ^{12}C, ^{14}N, or ^{16}O as well as elastic recoil on hydrogen and elastic scattering.

For example, carbon and hydrogen from a C$_x$H$_y$ coating can be analyzed simultaneously if we know the cross sections of the ^{12}C(^{3}He,p_0)^{14}N nuclear reaction and ^{1}H(^{3}He,^{1}H)^{3}He elastic recoil reaction. The cross section of the first reaction has been measured by different authors[1,2] while the cross section of the elastic recoil ^{1}H(^{3}He,^{1}H)^{3}He reaction has not yet been measured. Nevertheless, the cross section of the reverse nuclear reaction ^{3}He(^{1}H,^{1}H)^{3}He is known[3,4] in a range of energy higher than the energies usually chosen for depth profiling hydrogen (1–3 MeV). Theoretical studies of the ^{1}H(^{3}He,^{1}H)^{3}H reaction have also been done by extrapolating phase shift for ^{3}He energies below 3 MeV.[5]

II. STANDARD PREPARATION

Two silicon samples cut out of a silicon wafer [orientation (100)] were used as substrates. A thin film of α-SiC:H was deposited simultaneously onto these two substrates by means of plasma enhanced chemical vapor deposition (PECVD). The standards were transferred in air to the analysis chamber, in which the typical pressure was 2×10^{-8} mbar during the analysis. The composition of the SiC:H film was measured by means of Rutherford backscattering spectroscopy (RBS) on the SiC:H film. Details on the apparatus setup for the RBS measurements can be found in Ref. 6. The simulation was done with the GISA code.[7] The measured ratio was Si/C=0.50.

III. HYDROGEN PROFILING USING ERD $E \times B$ TECHNIQUE

The hydrogen depth profiles were measured in the same analysis chamber by means of the ERD $E \times B$ method described in detail earlier.[8] Briefly, a 350 keV (25 nA) ^{4}He$^+$ ion beam is incident at an angle of 65° with respect to the normal of the sample surface. A low-noise ion-implanted detector with a resolution of 7 keV [full width at half-maximum (FWHM)] is used to energy-analyze the H$^+$ recoils at an angle of 45° to the incident beam. The very large background of He$^{0,+,2+}$ is eliminated with the achromatic electromagnetic ($E \times B$) filter as described in Ref. 8. The beam current is measured by counting, in a second detector, the backscattered yield from a target consisting of tungsten spokes. This system is calibrated by means of a Faraday cup and the precision is estimated to ±2%.

The H$^+$ spectrum is corrected for the undetected H^0 (H^{-1} is negligible) fraction using the charge fractions measured accurately (±1%) previously.[9] The "total" (H^0+H$^+$) spectrum is deconvoluted into a depth spectrum with a computer code that uses the stopping powers of Ziegler and co-workers.

The depth resolution is mainly affected by the energy resolution of the detector δE_d, the energy straggling δE_s, and the multiple scattering δE_m. In our experimental conditions, all the other effects are negligible. Assuming noncorrelated processes and Gaussian distribution for the energy spreads, the total depth resolution is given by $(\delta E_L)^2 = (\delta E_S)^2 + (\delta E_S)^2 + (\delta E_m)^2$. Straggling and multiple scattering have been calculated as described in Ref. 11 and both increase with depth. The depth resolution depends on both the energy resolution and the energy loss (dE/dx). It has been plotted in function of depth and fitted by means of the equation $\delta^2 x = \delta^2 x_d + \delta x_{c1} x + \delta_{c2} x^2$, where $\delta^2 x_d$ is the detector contribution, and δx_{c1} and δ_{c2} are due to both multiple scattering and straggling contributions. Their values are given in Table I of Ref. 8 for different materials. For SiC, the values of $\delta^2 x_d$, δx_{c1}, and δ_{c2} are 10.2 nm^2, 0.845 nm, and 0.01, respectively.

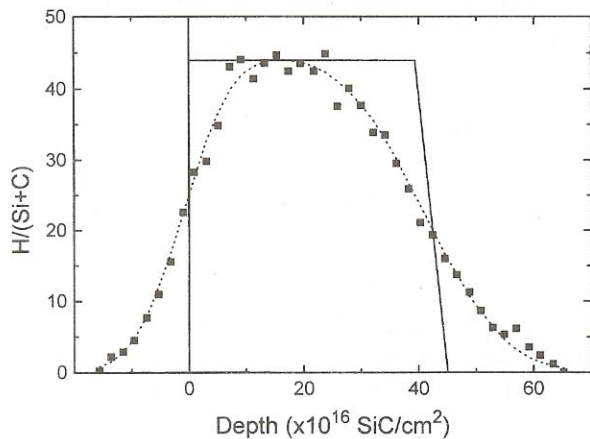[a)]Electronic mail: larn@quick.cc.fundp.ac.be

FIG. 1. Depth profiles of hydrogen included in the SiC:H layer, still resolution broadened (■), with the depth resolution subtracted (—) and a convolution of the real depth profile with the depth resolution function (···).

FIG. 2. The experimental setup with three particle detectors. The incident angle α is 10° for all measurements and β is set to 10° or 20°.

The measured depth profile (still resolution broadened) of hydrogen contained in the SiC:H layer is shown in Fig. 1. The depth resolution was subtracted[12] from this profile in order to obtain the real profile as shown in Fig. 1. Finally, the real depth profile was convoluted with the depth resolution function to check the validity of the procedure and the result is plotted in Fig. 1.

Special care was taken in order to be sure that no hydrogen depletion happened during the analysis. Measurements were repeated several times with different beam charges and currents, starting with very low fluences (10^{11} ^{4}He$^+$/cm^2). During all these measurements, the hydrogen remained very stable in the SiC:H layer. The composition of the standard is Si$_{0.23}$C$_{0.46}$:H$_{0.31}$ and the hydrogen content is 18.7×10^{16} H/cm^2.

IV. CROSS SECTION MEASUREMENTS OF THE ¹H(³He,¹H)³He ELASTIC RECOIL REACTION

A. Experimental details

We have measured the recoil cross section of the ^{1}H(^{3}He,^{1}H)^{3}He reaction between 1.9 and 3 MeV at two different angles (20° and 30°). The standard used for the measurement was the SiC:H layer described in the previous section. We have first verified the stability of hydrogen contents during the bombardment with high energy He beam. Hydrogen contents of 18.7×10^{16} H/cm^2 as measured with the conventional ^{1}H(^{4}He,^{1}H)^{4}He reaction using the ERD $E\times B$ technique (Sec. III) did not change during this bombardment.

Prior to the cross section measurement of the ^{1}H(^{3}He,^{1}H)^{3}He reaction, we have evaporated a very thin layer of gold (2.86×10^{15} atoms/cm^2) on the standard in order to normalize the results. The experimental setup is shown in Fig. 2. The ^{3}He beam was produced by a 2.5 MV Van de Graaff accelerator. Three detectors were placed in the analyzing chamber pumped down with a turbomolecular pump and the residual pressure was lower than 5×10^{-7} mbar. A liquid nitrogen trap was placed in the path on the incident particle in order to avoid carbon and hydrogen contamination during the irradiation. We have checked the carbon and hy-
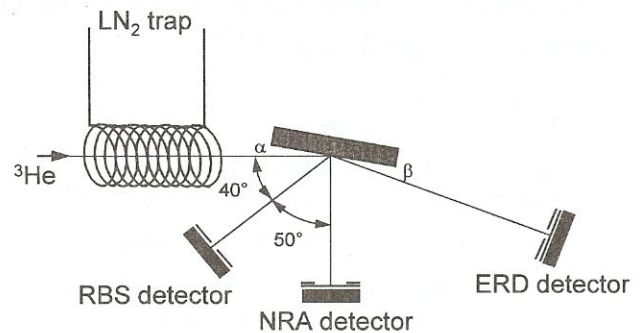
drogen contamination after a long irradiation time: we did not observe a surface contamination of carbon or a depletion of hydrogen during irradiation after the integration of 9 μC of ^{3}He particles (5 nA during 30 min). The first detector (PIPS detector), named ERD, was placed at 100 mm from the beam impact at 20° or 30° relative to the incident beam. An absorber foil of Al (12.5 μm) was placed in front of the detector and a rectangular slit (1 mm$\times$13 mm) defined a solid angle of 1.3 msr. The second surface barrier detector named NRA, was placed 70 mm from the beam impact at 90° relative to the incident beam. A circular collimator of 15 mm diam defined a solid angle of 36.1 msr and an absorber foil of aluminum (10 μm) was placed in front of the detector in order to stop the backscattered ^{3}He particles. Carbon contents of the standard was controlled by this detector using ^{12}C(^{3}He, p_i)^{14}N reactions. The third detector (PIPS), labeled RBS and placed at the backscattering angle of 140°, was used to measure the integrated beam charge with the signal due to the evaporated layer of gold on the standard. This detector was collimated with a 1.5 mm diameter hole showing a solid angle of 0.382 msr.

B. Results and discussion

Figure 3 shows typical spectra obtained simultaneously with the three detectors with 2.4 MeV ^{3}He particles incident on the SiC:H/Si standard. The number of incident particles will be the same for the three detectors because the information relative to gold in the RBS detector can be used for normalizing the data is we assume that the elastic cross section on gold follows the Rutherford law. The ERD spectrum taken at 20° [Fig. 3(a)] shows a Gaussian peak which is attributed to hydrogen recoiling from the SiC:H layer. The Gaussian shape of hydrogen peak is due to the fact that the experimental data are the convolution between the rectangular theoretical depth profile (Fig. 1), the straggling effect in the standard and the absorber foil, and the elastic recoil cross section.

The spectrum represented at Fig. 3(b) was recorded on the standard with the NRA detector in the same condition as the previous spectrum. We can observe the peaks relative to the ^{12}C(^{3}He,p_i)^{14}N nuclear reactions labeled ^{12}Cp_i($i=1,4$). The ^{12}Cp_1 peak overlaps the ^{16}Op_0 and ^{16}Oα_0 due respectively to ^{16}O(^{3}He,p_0)^{18}F and ^{16}O(^{3}He,α_0)^{15}O nuclear reac-
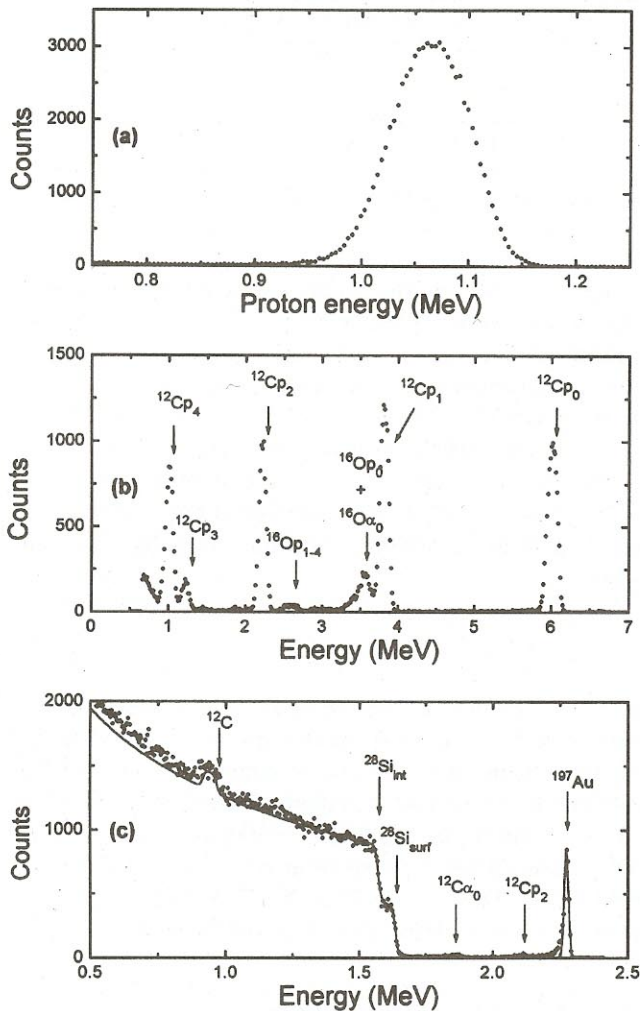
FIG. 3. (a) ERD spectrum obtained by bombardment of 2.4 MeV ³He particles on a SiC:H/Si standard. (b) spectrum recorded in the NRA detector in the same condition as in (a). The $^{12}Cp_i$ and $^{16}Op_i$ labeling of the peaks correspond to $^{12}C(^3He,p_i)^{14}N$ and $^{16}O(^3He,p_i)^{18}F$ reactions, respectively. (c) RBS spectrum of the same standard. The full line is the simulation with RUMP code with the data from Table I.

TABLE I. Analysis for the α-SiC:H film obtained using RUMP simulation code (Ref. 14).

Layer number	Thickness (10^{15} atoms/cm²)	Composition and atomic fraction
1	2.86	Au 1
2	571	Si 0.251 C 0.422 H 0.327
3	∞	Si 1

good. Nevertheless, we have to be careful with the peak relative to gold in order to avoid interference between $^{12}C(^3He,\alpha_0)^{11}C$ or $^{12}C(^3He,p_2)^{14}N$ nuclear reactions [small peaks labeled $^{12}C\alpha_0$ and $^{12}Cp_2$ in Fig. 3(c)] and $^{197}Au(^3He,^3He)^{197}Au$ elastic nuclear reaction, but the magnitude of the cross section of nuclear relations on ^{12}C is more than 10 000 times less than the elastic scattering on gold.

It is also quite clear that carbon as well as oxygen can be quantified only by means of the NRA detector because carbon and oxygen information in the RBS detector [Fig. 3(b)] interfere with the silicon from the substrate. Moreover, the elastic cross section $^{12}C(^3He,^3He)^{12}C$ or $^{16}O(^3He,^3He)^{16}O$ do not follow the Rutherford cross sections.

The differential cross section of the $^1H(^3He,^1H)^3He$ nuclear reaction is given by

$$\left(\frac{d\sigma}{d\Omega}\right)_{ERD} = \frac{\cos\theta\, I_H}{\Omega_{ERD} N_1 N_H}, \tag{1}$$

where θ is the angle between the incident beam and the normal of the sample; I_H is the integral or the area under the peak due to the nuclear reaction [Fig. 3(a)]; Ω_{ERD} the solid angle of ERD detector; and N_1 the number of incident particles and N_H the number of hydrogen atoms (1.87×10^{17} atoms/cm²). A similar formula can also be written for the cross section of the $^{12}C(^3He,p_i)^{14}N$ nuclear reaction or elastic nuclear reaction on gold, which give, for example,

$$\left(\frac{d\sigma}{d\Omega}\right)_{RBS} = \frac{\cos\theta\, I_{Au}}{\Omega_{RBS} N_1 N_{Au}}, \tag{2}$$

where I_{Au} is the area or integral under gold information [Fig. 3(c)]; Ω_{RBS} is the solid angle of the RBS detector; and N_{Au} is the number of gold atoms (2.86×10^{15} atoms/cm²); and the other values are defined above.

By dividing Eqs. (1) and (2), we have a very simple formula for the differential cross section of $^1H(^3He,^1H)^3He$ nuclear reaction, which is

$$\left(\frac{d\sigma}{d\Omega}\right)_{ERD} = \left(\frac{d\sigma}{d\Omega}\right)_{RBS} \frac{I_H}{I_{Au}} \frac{\Omega_{RBS}}{\Omega_{ERD}} \frac{N_{Au}}{N_H}. \tag{3}$$

A similar equation can also be written for determining the elastic recoil cross section relative to nuclear reactions $^{12}C(^3He,p_i)^{14}N$.

The elastic recoil cross section $^1H(^3He,^1H)^3He$ has been measured on the SiC:H/Si standard between 1.9 and 3.0 MeV at two different angles 20° and 30°. In both cases, the angle between the incident beam and the surface of the speci-

tions, that show a resonance at 2.370 MeV.[13] We have calculated carbon contents of the SiC:H layer knowing the cross sections of $^{12}C(^3He,p_0)^{14}N$ or $^{12}C(^3He,p_2)^{14}N$ reactions and we have obtained 2.42×10^{17} atoms/cm². Moreover, by measuring carbon contents during the excitation curve measurement, we can control the carbon contamination at the surface of the sample. The enhancement of carbon during irradiation can be neglected due to low residual pressure given by the liquid nitrogen trap placed in the path of the incident particles. We have also used carbon information in order to get the absolute recoil cross sections.

The spectrum shown in Fig. 3(c) is due to information recorded in the RBS detector during the same time as both previous detectors. Simulation has been done with RUMP code[14] in order to get the integrated charge on the sample. The result of the simulation is represented by the full line spectrum for a standard composition given in Table I and a total integrated charge of 14.5 μC. The agreement between the experimental data and the simulated spectrum is very

Terwagne, Ross, and Leblanc

FIG. 4. Differential cross sections for the $^1H(^3He,^1H)^3He$ nuclear reactions measured at 20°. The cross sections are measured relative to gold or carbon contents of the SiC:H/Si standard: (●) measurements relative to gold, (△) measurements relative to $^{12}C(^3He,p_0)^{14}N$ nuclear reaction, (◆) measurement relative to $^{12}C(^3He,p_1)^{14}N$ nuclear reaction, and (×) measurements relative to $^{12}C(^3He,p_2)^{14}N$ nuclear reaction. The full line is the theoretical cross section given in Ref. 5 and the dotted line is the polynomial fit done in the cross sections measured relative to gold.

men was 10°. The results are presented in Figs. 4 and 5. We have presented in Figs. 4 and 5 the measurement of the cross section relative to Au as well as the results relative to C. We can observe a very good agreement in the range 2.0–2.7 MeV between all the measurements, but a disagreement at low energy (under 2.0 MeV) and at high energy. At low energies, the cross sections of the $^{12}C(^3He,p_i)^{14}N$ nuclear reactions are very low[2] and the errors on the calculated cross sections relative to C are higher than 15%. At higher energies (>2.8 MeV), the $^{12}C(^3He,p_i)^{14}N$ cross sections decrease rapidly,[2] which leads to a lower cross section for the elastic recoil reaction. For those reasons, we have decided to keep only the data relative to gold (dots). The absolute error on
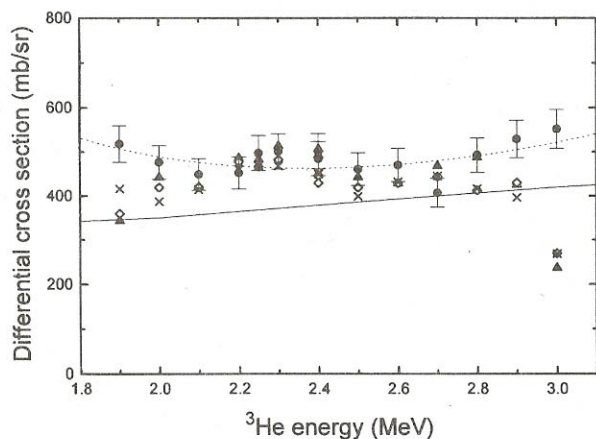

FIG. 5. Differential cross sections for the $^1H(^3He,^1H)^3He$ nuclear reactions measured at 30°. The cross sections are measured relative to gold or carbon contents of the SiC:H/Si standard: (●) measurements relative to gold, (△) measurements relative to $^{12}C(^3He,p_0)^{14}N$ nuclear reaction, (◆) measurements relative to $^{12}C(^3He,p_1)^{14}N$ nuclear reaction, and (×) measurements relative to $^{12}C(^3He,p_2)^{14}N$ nuclear reaction. The full line is the theoretical cross section given in Ref. 5 and the dotted line is the polynomial fit done in the cross sections measured relative to gold.

TABLE II. Optimal values for the coefficients C_i from formula 4 obtained by least-squares fits to the experimental cross sections.

θ (deg)	C_{-1}	C_0	C_1	C_2
20	1.3657	0.0269	7.0730	−0.4577
30	1.0705	0.5529	8.4432	2.8995

the cross sections $^1H(^3He,^1H)^3He$ measured relative to gold is due to three different factors [Eq. (3)]: statistical errors on the determination of I_H and I_{Au} (3%), systematical errors on the measurements of the solid angles Ω_{RBS} and Ω_{ERD} (2%), and experimental errors due to the measurement of N_H and N_{Au} (4%). The overall error has been estimated to be less than 8%. We have reported the error bars on Figs. 4 and 5.

A polynomial fit of the experimental cross sections has been done with an arbitrary function given by Tirira and Bodart:[15]

$$\ln\left(\frac{d\sigma(E_{He},\theta)}{d\Omega}\right) = C_{-1}E_{He} + C_0 + C_1 E_{He}^{-1} + C_2 E_{He}^{-2}, \quad (4)$$

where the coefficients C_i given in Table II represent the optimum values of the least-squares fits to the experimental cross sections measured relative to gold (Figs. 4 and 5). The results of the polynomial fit is represented by the dotted lines on Figs. 4 and 5. We have also reproduced the theoretical cross sections given by Benenson et al.,[5] which are represented by the full lines in Figs. 4 and 5. Theoretical cross sections are always lower than the experimental one.

V. EXAMPLES OF APPLICATION

Our new technique for profiling simultaneously hydrogen and carbon has been applied in two cases. The first sample is a silicon wafer implanted with 1.5 keV H^+. The retained dose of hydrogen (3.6×10^{16} atoms/cm^2) has been measured using the ERD $E \times B$ technique and the depth profile is shown in Fig. 6 (dashed line). We have also measured the depth profile of hydrogen using the $^1H(^3He,^1H)^3He$ elastic recoil technique and the results are also presented in Fig. 6. A retained dose of 3.74×10^{16} H/cm^2 has been measured. The difference between hydrogen contents obtained by the two techniques is less than 4%. We can observe a small difference in the thickness of both profiles due to the fact that the depth resolution of the ERD $E \times B$ technique is better than the resolution obtained by the $^1H(^3He,^1H)^3He$ elastic recoil reaction.

The second example is a more complex multilayer. We deposited by DC-magnetron sputtering technique three different layers on a silicon substrate. The first layer was 500-Å-thick C_xH_y deposited on a silicon wafer; a second layer of copper (thickness 500 Å) and a third layer similar to the first one were then deposited. The multilayer consists of a $C_xH_y/Cu/C_xH_y/Si$ sample. We have measured the hydrogen profile with ERD at 20° as well as NRA and RBS spectra. The result is shown in Fig. 7. Figure 7(a) shows two peaks due to recoil of hydrogen from the C_xH_y layers. This spectrum is the sum of 20 spectra recorded successively in order

J. Appl. Phys., Vol. 79, No. 12, 15 June 1996
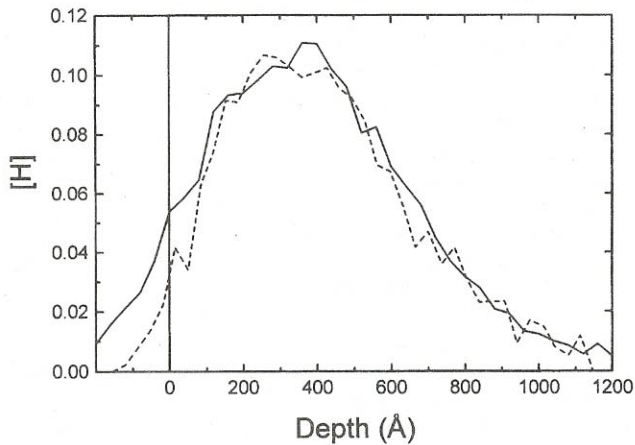
Terwagne, Ross, and Leblanc   8889

FIG. 6. Depth profiles of hydrogen implanted into silicon at low energy (1.5 keV); a retained dose of hydrogen (3.6×10^{16} atoms/cm^2) has been measured using the ERD $E \times B$ technique (- - -). The depth profile of hydrogen using the ^{1}H(^{3}He,^{1}H)^{3}He elastic recoil technique is represented by the solid line and the retained dose measured is 3.6×10^{16} atoms/cm^2.

to follow hydrogen migration during irradiation. Hydrogen stays in place during irradiation and we conclude that no migration is due to irradiation. We have also observed that copper is free from hydrogen. We have simulated the spectrum with ALEGRIA code[16] and we found 1.82×10^{17} H/cm^2 in the first layer and 2.02×10^{17} H/cm^2 in the second one assuming a mean stopping power (Al) for the whole sample. For that specimen, we did not evaporate a thin gold layer on the specimen because copper information recorded in the RBS detector [Fig. 7(c)] can be used for measuring the incident charge. We have simulated the RBS spectrum using data of Table III with RUMP code[14] and we have compared the simulation (line spectrum) with the experimental spectrum. The agreement between the two spectra is very good. The big advantage of our new technique is the simultaneous measurement of carbon, hydrogen, and heavier elements like copper with the RBS detector. We can clearly observed in Fig. 7(b) the contribution of both carbon layers in the $^{12}Cp_2$ and $^{12}Cp_1$ peaks due, respectively, to ^{12}C(^{3}He,p_2)^{14}N and ^{12}C(^{3}He,p_1)^{14}N nuclear reactions. The contribution of both carbon layers is not so easily observable on the $^{12}Cp_0$ peak due to ^{12}C(^{3}He,p_0)^{14}N nuclear reaction. A shoulder can be seen at the left of the $^{12}Cp_0$ contribution. The line spectrum from Fig. 7(b) is the result of the simulation with SENRAS code using the data from Table III. The agreement between experimental and simulation spectra is also very good.

VI. CONCLUSIONS

The cross sections of the ^{1}H(^{3}He,^{1}H)^{3}He reaction have been measured at two different angles (20° and 30°) for ^{3}He particles incident energies between 1.9 and 3.0 MeV. This reaction offers a powerful alternative for profiling hydrogen to the classical ^{1}H(^{4}He,^{1}H)^{4}He elastic recoil reaction because ^{3}He incident particles induce nuclear reactions on light elements such as ^{12}C, ^{14}N, or ^{16}O as well as elastic recoil of hydrogen. The cross section is higher for the ^{1}H(^{3}He,^{1}H)^{3}He
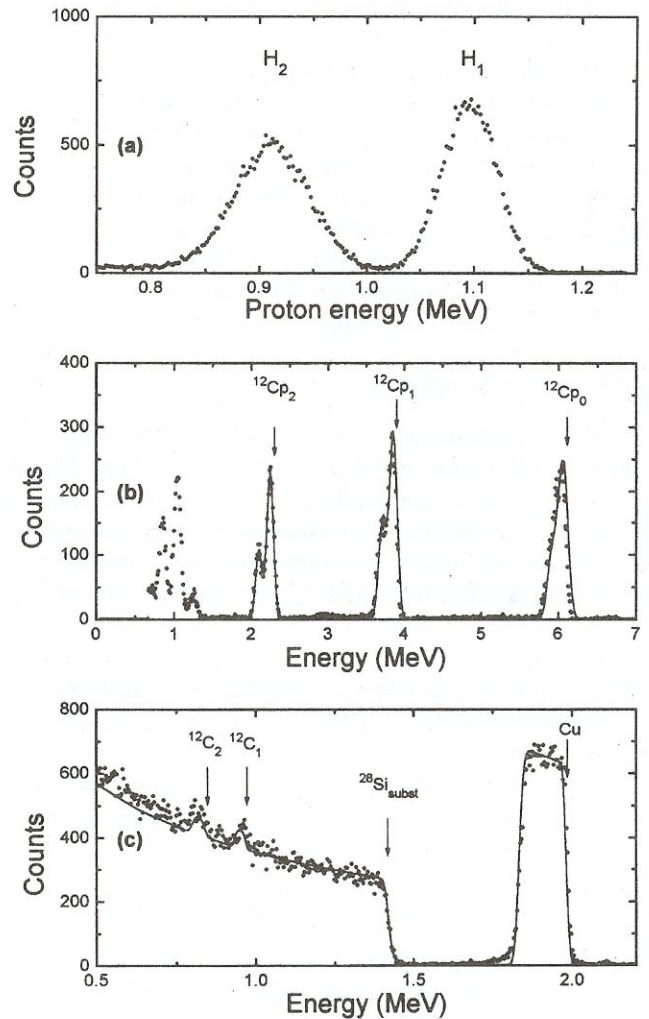
FIG. 7. (a) ERD spectrum obtained by bombardment of 2.4 MeV ^{3}He particles on a C$_x$H$_y$/Cu/C$_x$H$_y$/Si multilayer. The peaks labeled H$_1$ and H$_2$ are due, respectively, to hydrogen in the two C$_x$H$_y$ layers. (b) Spectrum recorded in the NRA detector in the same condition as in (a). The $^{12}Cp_i$ labeling of the peaks corresponds to ^{12}C(^{3}He,p_i)^{14}N reactions (i=0,1,2). The line spectrum is the result of the simulation with SENRAS code using the data from Table III. (c) RBS spectrum of the same multilayer. The peaks labeled ^{12}C$_1$ and ^{12}C$_2$ are due, respectively, to carbon in the two C$_x$H$_y$ layers. The full line is the simulation with RUMP code with the data from Table III.

TABLE III. Analysis for the C$_x$H$_y$/Cu/C$_x$H$_y$/Si multilayer obtained using RUMP simulation code (Ref. 14).

Layer number	Thickness (10^{15} atoms/cm^2)	Composition and atomic fraction
1	414	C 0.54 H 0.46
2	407	Cu 1
3	450	C 0.55 H 0.45
4	∞	Si 1

reaction than for the $^{1}H(^{4}He,^{1}H)^{4}He$ elastic recoil reaction. We give an analytical formula for the cross section measured in this paper.

This new technique has been applied to silicon implanted with low energy hydrogen and gives results in very good agreement with the more classical ERD $E \times B$ technique. Moreover, carbon and hydrogen and copper from a multilayer like $C_xH_y/Cu/C_xH_y$ on silicon has been measured together. Combining Rutherford backscattering spectroscopy, nuclear reaction analysis, and elastic recoil detection, light and heavy elements can be simultaneously analyzed with a good depth resolution.

ACKNOWLEDGMENTS

[1] S. Y. Tong, W. N. Lennard, P. F. A. Alkemade, and I. V. Mitchell, Nucl. Instrum. Methods B **54**, 91 (1990).

[2] G. Terwagne, Nucl. Instrum. Methods B (to be published).

[3] T. A. Tombrello, C. Miller Jones, G. C. Phillips, and J. L. Weil, Nucl. Phys. **39**, 541 (1962).

[4] W. E. Meyerhof and T. A. Tombrello, Nucl. Phys. A **109**, 1 (1968).

[5] R. E. Benenson, L. S. Wielunski, and W. A. Lanford, Nucl. Instrum. Methods B **15**, 453 (1986).

[6] G. G. Ross, L. Leblanc, B. Terreault, J. F. Pageau, and P. A. Gollier, Nucl. Instrum. Methods B **66**, 17 (1992).

[7] J. Saarilahti and E. Rauhala, Nucl. Instrum. Methods B **64**, 734 (1992).

[8] G. G. Ross, B. Terreault, G. Gobeil, G. Abel, C. Boucher, and G. Veilleux, J. Nucl. Mater. **128/129**, 730 (1984); G. G. Ross and L. Leblanc, Nucl. Instrum. Methods B **62**, 484 (1992).

[9] G. G. Ross and B. Terreault, Nucl. Instrum. Methods B **15**, 146 (1986); G. G. Ross and L. Leblanc, *ibid.* B **48**, 134 (1990).

[10] H. H. Andersen and J. F. Ziegler, *Hydrogen Stopping Powers and Ranges in All Elements* (Pergamon, New York, 1977); J. F. Ziegler, *Helium Stopping Powers and Ranges in All Elements* (Pergamon, New York, 1977).

[11] L. Leblanc, G. G. Ross, and B. Terreault, INRS-Energie, Report No. NRG-609 (in French); G. G. Ross and B. Terreault, Nucl. Instrum. Methods B **15**, 61 (1986).

[12] F. Schiettekatte, R. Marchand, and G. G. Ross, Nucl. Instrum. Methods B **93**, 334 (1994).

[13] F. Abel, G. Amsel, E. d'Artemare, C. Ortega, J. Siejka, and G. Vizkelety, Nucl. Instrum. Methods B **45**, 100 (1990).

[14] L. R. Doolitlle, Nucl. Instrum. Methods B **9**, 344 (1985).

[15] J. Tirira and F. Bodart, Nucl. Instrum. Methods B **74**, 496 (1993).

[16] F. Schiettecatte, A. Chevarier, N. Chevarier, A. Plantier, and G. G. Ross, in Proceedings of IBA'12 (unpublished).